Non-destructive determination of core-transition-outer wood of *Pinus nigra* combining FTIR spectroscopy and prediction models

René Herrera [a],[*], Eva Hermoso [b], Jalel Labidi [a], Juan I. Fernandez-Golfin [b]

[a] *University of the Basque Country (UPV/EHU), Chemical and Environmental Engineering Department, San Sebastián, Spain*
[b] *Forest Products Department, INIA-CIFOR-CSIC, Madrid, Spain*

ARTICLE INFO

ABSTRACT

The early detection of wood quality by using advanced analytical non-destructive methods is an ongoing area of research and is highly interesting for the forest-based sector. The presence of core wood has negative effects on the performance of this material; hence, it is essential to identify this region as well as to define the endpoint where the region defined as transition wood begins. The purpose of this study was to apply a novel methodology for wood quality classification, based on FTIR spectroscopy, in combination with chemometrics, generating models capable of differentiating and predicting core wood, transition, and outer wood of Pinus nigra. This study also attempts to classify which specific IR bands define the chemical differentiation of woody regions. The results of the predictive models generated were satisfactory, attaining a full identification of classes with a non-linear SVM-DA model showing higher correlation coefficients than the generated linear SIMCA and PLS-DA models. SIMCA and PLS-DA were suitable for bands contrast and for categorizing the IR fingerprint in relation to the core-transition-outer regions. This study presents discriminative models generated from a non-destructive and relatively fast IR methodology with high correlation coefficients, thus improving the existing methods that are currently practiced for identifying wood quality. However, the database requires progressive calibration and adjustments to have acceptable reliability when validating the methods over time.

1. Introduction

Wood is a complex biological structure developed over millions of years to aid water conduction, mechanical support, and storage of biochemicals in trees. Different biochemical combinations define physical, mechanical, chemical, and biological properties of each species and, from a technological point of view, define the wood quality. The particular way in which trees grow generates changes over time in ring width and density, early and late wood formation, and in the core (also identified as juvenile wood), transition, and outer (also identified as adult wood) wood proportions [1,2].

The core wood corresponds to the inner part of the trunk near the pith and optically present wider yearly rings. It has a cellular structure with lower tracheid length, reduced density, stiffness, and cellulose/lignin ratio, but higher spiral grain and microfibril angle [3]. The presence of corewood negatively affects the final products by reducing their mechanical and structural properties; hence, it is essential to identify and quantify this region as well as to define the end point where

the region defined as transition wood begins.

In practice, the core wood is designated as the first 10 rings from the pith to the bark; from this point to about the 15th ring is the transition part, and from the 16th ring onwards is the outer wood [4–6]. However, the current procedure used for that purpose is mainly based on visual verification, requiring alternative procedures capable of identifying the presence of core-transition-outer wood with greater precision and preferably by using repeatable non-destructive methodologies.

Various studies have been conducted to determine the point of demarcation between inner-outer wood using different methodologies. These include the use of specific gravity data, where linear regressions, segmented regression or discriminant analysis are widely used to determine the demarcation point [7–10]. In addition, the measurement of the cellulose microfibril angles (MFA) is also used to describe the core-outer wood, as it provides useful information to distinguish regions of the wood, since the MFA are large in the core wood and small in the outer wood [11,12].

Moreover, methods that combine X-ray diffraction techniques with

---

* Corresponding author.
E-mail addresses: renealexander.herrera@ehu.eus (R. Herrera), hermoso@inia.csic.es (E. Hermoso), jalel.labidi@ehu.eus (J. Labidi), golfin@inia.csic.es (J.I. Fernandez-Golfin).

computer tomography could create density profiles with good accuracy by analyzing anatomical properties and changes in density according to the cellulose MFAs [13,14] or associating annual shrinkage variations to corewood and outerwood areas segregation [15]. The main drawbacks of these methods at laboratory conditions are the time-consuming and laborious sample preparation, making their inclusion in projects that involve large numbers of samples, such as genetic studies or breeding programs, impractical [16]. These facts contribute towards the ongoing exploration of alternative non-destructive methods to identify wood quality such as the Near Infrared-Hyperspectral Imaging (NIR-HI) as an alternative technique to X-ray densitometry [17].

Another alternative method is to measure the spectroscopic signals in the infrared region that capture chemical information by converting the beam of infrared light directed towards wood in vibrational data related to its molecular structure, chemical bonds, and combined bands. From the acquired information, it is possible to differentiate the chemical composition of a large number of samples, with the advantage of using a non-destructive technique for wood analysis [18–20]. Fourier transform infrared (FTIR) spectroscopy has been described as a tool to study the chemistry of wood as well as the changes caused by diverse wood modification processes [21]. FTIR spectrum is, therefore, a superposition of several absorption peaks that are interpretable with band assessment tables previously published by several authors [22–25].

However, the best practice to extract relevant chemical information of a FTIR dataset is in terms of approximate statistical and mathematical models known as chemometrics. A chemometric model describes variability around the chemical model by separating the noise from the data, thus obtaining chemically relevant information to represent a set of uncorrelated linear combinations of the original variables that contain most of the variability of the dataset [24–26]. In particular, the FTIR associated with multivariate modelling approach such as principal component analysis (PCA), clustering algorithms, or regression analysis including partial least squares (PLS) and PC-regression could be used for the identification and characterization of wood samples [27].

This study focused on *Pinus nigra* Arn. Subsp.Salzmannii which is a Mediterranean coniferous species widely distributed in Spain (352,954 Has), with an estimated sawn wood production of 310,000 m^3/year and of particular interest for structural purposes due to its high mechanical performance [28]. The objective of this study is to create a novel methodology of wood classification based on FTIR spectroscopy in combination with chemometrics, generating models capable of differentiating and predicting core wood of transition and outer wood of *Pinus nigra*. The results obtained could also help to understand and classify which specific IR bands influence the differentiation of woody regions of this coniferous species.

2. Materials and methods

2.1. Geographic origin of wood and sampling procedure

The wood material was selected from twelve individual trees of black pine (*Pinus nigra* Arn. Subsp.Salzmannii), approximately 55 years old, planted in Zarzuela de Jadraque, Guadalajara, Spain (41°1́N, 3°4́W) at an altitude above 1000 m (a.s.l.) on a flat area (1–10% slope in NW direction). Based on a 50-year historical series (1962–2012), the meteorological data of this area shows that the average annual temperature was 10.6 °C, and the average annual rainfall was 493 mm (AEMET 2022).

For the data collection, wooden discs at heights of about 1.3 m and 4.3 m were cut into radial profiles (pith to bark including core-transition-outer wood), and then kept at low temperature (4 °C) until evaluation. To assure equal moisture content during the testing process, the profiles were first freeze-dried until constant weight, and then conditioned in a climate chamber at 65% relative humidity and 25 °C until constant weight (equilibrium moisture). Samples were kept in these conditions until further analysis.

To minimize inaccuracy during the spectral measurements, sampling was done in the same way for all samples. First, samples were prepared by sanding and planning the surfaces using a belt sanding machine with an abrasive paper P120 on the transverse and longitudinal face of the samples, reducing with that the possible variations due to the roughness of the material. Furthermore, after considering the simplicity, less time consuming, and homogeneity, the spectral information was acquired each 5 mm in the transverse and longitudinal face from the pith towards the bark.

2.2. Testing procedure and equipment

Ten profiles without visible defects (such as resin channels, knots, or discoloration) were selected taking a minimum of 30 individual measurements on the transverse and longitudinal face of the samples and was used as calibration set. The type of wood was identified from the pith to bark direction as follows: core (1–10 scans) transition (11–15 scans), outer wood (16–30 scans). In addition, six profiles from another collection were analyzed by using the same methodology (validation set).

The wood profiles were scanned in the spectral range between 4000 cm^{-1} to 400 cm^{-1} with 4 cm^{-1} of resolution and accumulating 32 scans. A Spectrum Two FT-IR Spectrometer with Attenuated Total Reflectance (L1050231Universal ATR, Perkin-Elmer, Waltham, MA, USA) was used to scan the samples. The average spectral data of each measurement (32 scans) was used for the chemometric analysis. Each spectrum was obtained by applying a constant gauge pressure during each measurement for intimate contact onto the ART crystal (internal reflection element). The diamond crystal was cleaned with ethanol before rescanning.

2.3. Data preprocessing

In order to maximize information content and minimize noise, the spectral data was adjusted and corrected (Table 1). The standardization process started by cutting from the raw spectra the fingerprint spectral region (750–1850 cm^{-1}), then smoothing the signals using a mild Savitzky-Golay filtering algorithm, and finally removing the baseline offsets from data using the weighted least squares method (WLS). Different filtering methods were used: calculating the derivatives (1st-2nd derivative according to the Savitzky-Golay algorithm) or correcting the scattering of light by Extended Multiplicative Scatter Correction (EMSC). Moreover, signals were normalized according to the standard normal variate (SNV) method, and the signal to noise ratio (SNR) was adjusted to 3–5 eigenvectors within the threshold.

2.4. Data analysis

After signal preprocessing the database was classified based on where they were measured naming them as core-transition-outer wood, and randomly distributed into the data matrix to avoid linearity. The spectral information generated was divided into two different data series, one to perform the calibration and another for the validation of the models.

The preliminary sample discrimination was evaluated with the unsupervised methods hierarchical cluster analysis (HCA) and principal component analysis (PCA). HCA was used to identify sections that have a similar spectral response by clustering the spectra to reduce intra-cluster responses while maximizing the inter-cluster differences [28]. The first derivative of the FTIR spectra in the region 900–1800 cm^{-1} was selected for clustering using the Ward's method and the correlation coefficient as distance metrics algorithms. The results were plotted as dendrograms showing data distribution and optimal distance among clusters (heterogeneity).

Subsequently, the individual spectrums were distributed in 3 classes according to the vibrations and absorptions found in specific functional groups: the first class was distributed from 925 to 1145 cm^{-1}

Table 1

Summary of signal preprocessing methods and parameters obtained.

Wavelength (cm^{-1})	Wave range (%)	Smoothing (SavGol)	Filtering methods	Normalization	SNR	Factors
Raw data 400–4000	100	5	Baseline: WLS Filtering: 1st-2nd derivative -	SVN	4	25
Adjusted data 925–1650	40	2	Baseline: WLS Filtering: EMSC	SVN	4	5

(dominated by carbohydrate-associated bands), the second class from 1487 to 1553 cm^{-1} (dominated by aromatic skeletal vibrations), and the third class from 1553 to 1633 cm^{-1} (dominated by aromatics and extractives).

The data set-up was used for the exploratory method of PCA, which reduces the spectral set by decomposing a linear combination of original variables into a few principal components that contain the most variability in the dataset needed to determine differences among samples. PCA could allow the identification of bands with similar variability and support the identification of common precursors.

For the classification modelling supervised linear and non-linear methods were evaluated. The first approach was the use of independent modelling of class analogy (SIMCA) method which is a linear method using principal components (PCs) as factors [29]. Moreover, partial least-squares discriminant analysis (PLS-DA) which is another linear method was also evaluated. In this case the discrimination of classes is done with latent variables as factors [30,31]. Finally, the non-linear method support vector machine analysis (SVMA) was tested, and the model compared with the linear strategies.

The results of the calibration test were contrasted with the validation set based on their statistical results and by using confusion matrix tables. PLS-Toolbox analytical software (Eigenvector research incorporated) was used for signal processing, data analysis and optimization of the most adequate configurations.

3. Results and discussion

3.1. IR spectra processing and exploratory classification

The set of samples for model calibration provided interpretable spectra over the adjusted fingerprint region (925–1650 cm^{-1}), which contains a selected number of bands that are indicative of the presence of the main chemical components of wood (Fig. 1a). From this set, a cluster analysis was conducted to determine if the spectral differences were sufficient to permit grouping of samples based on the wood designation (core (C)- transition (T)- outer (O)). The cluster results displayed two major well-separated clusters corresponding to the core-outer wood, two slightly separated clusters correlated to transition wood and one additional not correlated subcluster (Fig. 1b). The misclassified samples could be interpreted as the average error when a visual assessment (pith to bark direction) is performed. To improve the classification, the misclassified samples were revised, and the classes were reassigned for the following evaluations (Fig. 1c).

3.2. Exploratory unsupervised PCA results

The visualization of natural clustering in the processed IR spectra was explored by an unsupervised PCA analysis allowing for observation of how well the assigned classes (dominated by carbohydrate-associated bands, by aromatic skeletal vibrations or by aromatics and extractives) were distributed. The classification results in the PCA of the whole region were lower (925–1650 cm^{-1}) (RMSECV: 0.060) than when they were separated and analyzed in three independent PCAs (RMSECV: 0.054 to 0.011), thus applying a more precise bonding of spectral bands
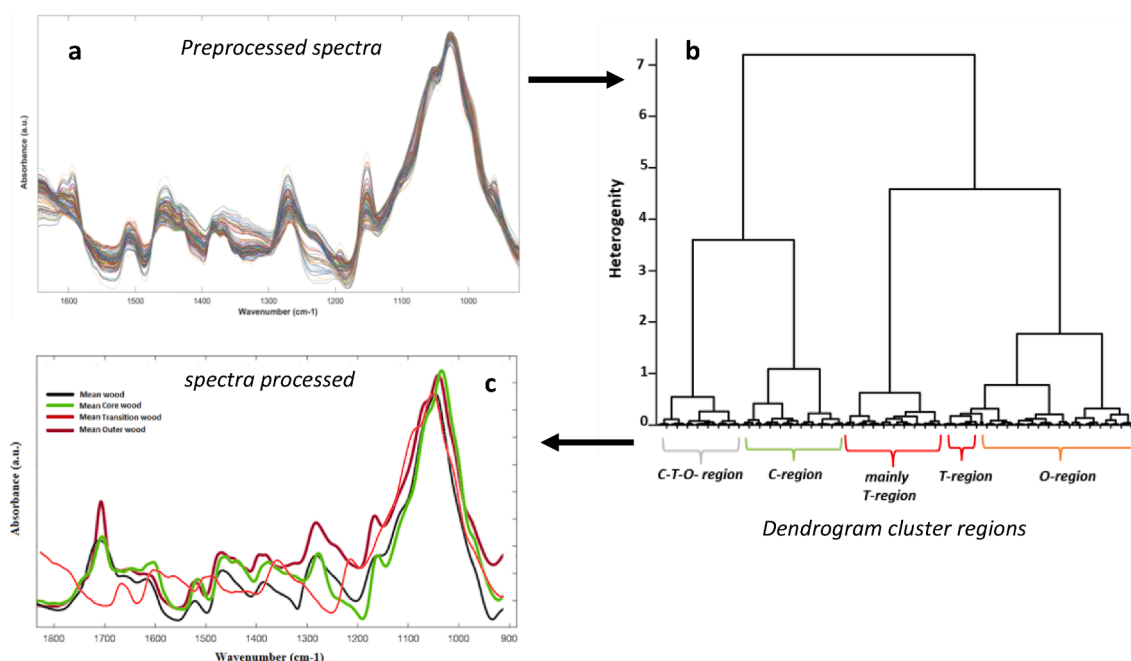

Fig. 1. FT-IR spectra preprocessing and exploratory cluster classification.

and regions especially in PCs with greater divergence as well as removing outliers. (Fig. 2). Subsequently, the set of samples were filtered (baseline, derivative or EMSC) and normalized (SNV), in which the best results reduced the spectra into 3–5 PCs including 99.77–99.81% of the cumulative variance (Table 2).

3.2.1. Exploratory PCA optimization

The PCA obtained after the spectral optimization showed improved results (4 PCs; RMSECV: 0.029) and important differences in specific bands and regions (Fig. 2). It should be noted that the most divergent wavenumbers on each region were identified by plotting PC's-loadings, acquiring information on specific active bands as well as reducing the overlapping of bands. The PC1-loading plot has a similar pattern to the average spectra and for that reason it was not considered further for discrimination and bands identification. PC2-PC3-PC4-loadings revealed clear differences from the original spectra, allowing visualization of overlapped bands and their relative intensity that diverges from the original spectrum (Fig. 2). Although PC3-PC4 accumulate < 1% of the spectral information they present the higher scores fitting in the reduced statistical threshold (0–1) and represent a more accurate separation of core-transition-outer classes. Loadings in PC2-4 show interesting bands corresponding to ring vibrations of different functional groups related to polysaccharidic compounds (bands around 1110 cm^{-1}, 1030 cm^{-1} and 950 cm^{-1}), aromatic compounds (bands around 1465 cm^{-1}, 1375 cm^{-1}, 1270 cm^{-1} and 1230 cm^{-1}), and related to different functional groups (bands around 1595 cm^{-1}, 1550 cm^{-1} and 1510 cm^{-1}).

3.3. Class modelling strategies

3.3.1. Supervised linear classification modelling

The SIMCA model was applied to classify the wood profiles based on an independent analysis of the principal components for each class (core-transition-outer) in a common multidimensional matrix. The model was built combining the resulting fitted classes to obtain a matrix of core (2PCs)-transition (2PCs)-outer (4PCs). Fig. 3 illustrates the Hotellings T2 *versus* Q residuals, which helps to explain how precise the model was in describing a given class (core-transition-outer). The samples belonging to the assigned classes fit within the 95% Qlimit, which was a good indicator of the model performance. Moreover, it was clear the discrimination of classes from the Qlimit distance on each evaluated class (Fig. 3), especially in the outer wood class where samples belonging to transition and core wood, were quite far from the reduced

limits of classification.

The results of the predictive model in general were satisfactory (Table 3), none of the core-outer wood exceeds the strict threshold (0.50) on the validation set of samples (unknown samples) attaining a full identification of those classes. Although core wood discrimination was 100% effective and the transition wood identification was acceptable, 70% of transition wood class were marked as unassigned in the predicted results. Even though the predicted results were quite precise, the model results show a high ratio of true/false or positive/negative scores in the discrimination of transition wood [30].

The second linear method applied was the PLS-DA, providing models with lower within-class variability and maximized class-separation. The PLS-DA model was calibrated with 8 latent variables correctly classifying core-transition-outer wood with high coefficients of determination (Rc2) and small values of the cross-validation error (RMSEcv), thus providing a robust model with values between 0.83 and 0.92 and an error lower than 0.13. (Table 4).

The calibration set exhibited perfect scores within the strict threshold (0.50) and without misclassified core-transition-outer wood. The samples from the validation set were mostly classified correctly; however, the model efficiency was reduced to a coefficient of determination between 0.66 and 0.85 mainly due to misclassification of transition wood, which increased the error to 0.21. In general, the overall performance of the PLS-DA model outperformed that of the SIMCA model, which is also in accordance with several studies showing improved classification rates in the PLS-DA compared with SIMCA models [29–32].

To understand how well the PLS-DA model separates samples in a given class, from those not in class, sensitivity/specificity plots (thresholds plots) and the Receiver Operating Characteristics Curve (ROC curve) are shown in Fig. 4. Regarding the sensitivity/specificity plots for each class model (core-transition-outer wood), differences in the threshold distance were observed among classes, in core wood the lines cross while still at a value 1 (perfect class separation) but in the transition-outer wood the threshold varies in distance between estimated vs cross validated values, meaning that the number of predicted false negative values increased in the core class and the predicted false positive/negative was higher in the transition class.

These results also contrasted with the ROC curves (Fig. 4b) which expose similar information in a different format, thus allowing for the observation of differences between the curves of core wood class (with no false positives, no false negatives) and the dropping of the sensitivity/specificity plots in transition-outer classes as well as changes in the
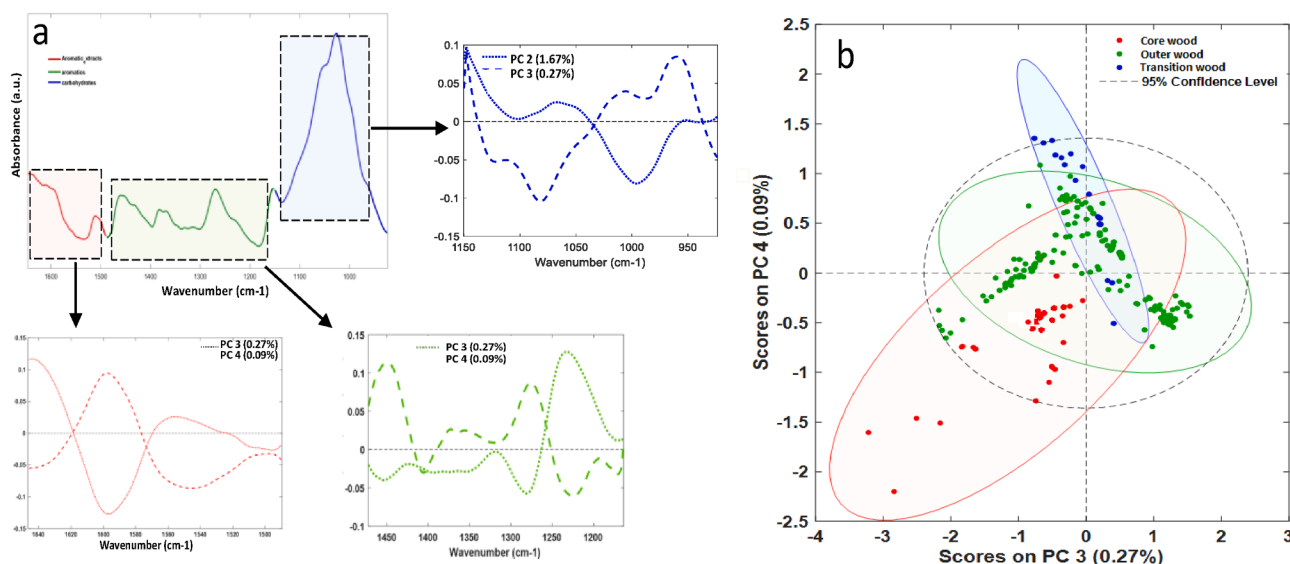

Fig. 2. Original spectrum, loadings and PCA scores.

Table 2

Summary of the PCA results in the whole spectra and in separated classes.

Spectral region (cm^{-1})	Relative wavelength percentage	Data preprocessing	PC's	% Cumulative variance	RMSEC	RMSECV
925–1650 (All)	100	Baseline-EMSC- SVN	5	99.77	0.0481	0.0601
Analysis of individual class groups						
1500–1650 (mainly aromatics)	20.8	Baseline-EMSC- SVN	5	99.81	0.0431	0.0546
1150–1500 (aromatics-carbohydrates)	48.6		4	99.80	0.0443	0.1137
925–1145 (mainly carbohydrates)	30.6		3	99.81	0.0434	0.0549
Analysis of whole spectral group						
925–1650 (all adjusted)	100	Baseline-EMSC- SVN	4	99.95	0.0233	0.02939

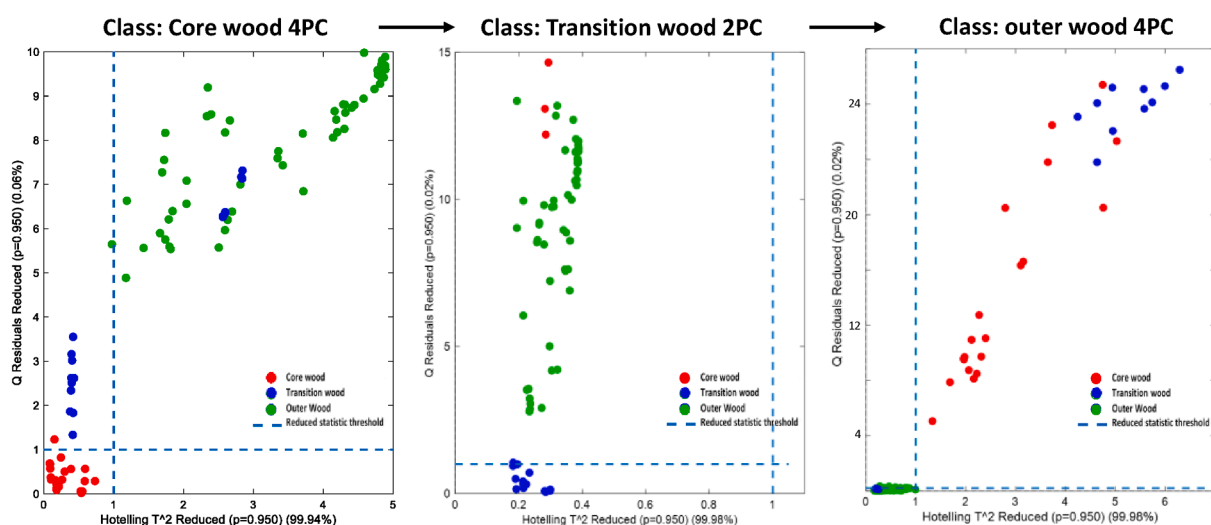PC = principal components.

Fig. 3. Class discriminations results (Hotellings T2 *versus* Q residuals).

Table 3

Results of the predictive discriminative SIMCA model.

SIMCA MODEL[a] Class	Model results			Prediction results		
	TPR	FNR	Error	TPR	FNR	Error
Core	1.0000	0.0000	0.0000	1.0000	0.0000	0.0000
Transition	0.7000	0.3000	0.0349	0.2857	0.7143	0.0349
Outer	0.9831	0.0169	0.1163	1.0000	0.0000	0.0000
Confusion table	**Model results**			**Prediction results**		
	core	transition	outer	core	transition	outer
Predicted as core	**170**	0	0	**60**	0	0
Predicted as transition	0	**70**	0	0	**20**	0
Predicted as outer	0	0	**580**	0	0	**300**
Unassigned	0	30	10	0	50	0

[a] Classification rule: prediction strict (0.50). TPR: true positive ratio FNR: false negative ratio.

model threshold. The results suggest including small improvements in the discrimination of transition and outer classes in such a way that the true positives (sensitivity) and true negatives (specificity) will be maximized.

3.3.2. Supervised non-linear classification modelling

The latter model was created using the Support Vector Machine (SVM-DA), a supervised discriminant method which produce linear boundaries between object groups in a much higher dimension than the original x-space. SVM did not try to model classes of objects since the method identifies the classes if the result of the function is < 1 or −1, obtaining a range of reinforcement values ([-1,1]) that acts as a margin between classes [33]. Model results and predicted values are presented in Table 5..

The optimal parameters of SVM-DA model were set with the kernel function (radial basis function), cost function (100), gamma function (0.31), and the threshold used to estimate the classes was 0.5. The results of the predictive model were satisfactory, none of the core-outer wood exceeded the strict threshold (0.50) reaching a full identification of classes on the validation set of samples. An additional cross-validation (CV) based parameter was included in the results to figure out details of the model that are not visible on the self-prediction classifications (model results). The results showed a slight decrease in the sensitivity/ specificity in the transition-outer classes that were not observed in the predictive results. This additional cross-validation is useful for model optimization and could be considered as the error estimate on the final selected model to reduce false classifications.

In general, the SVM-DA model to identify core-transition-outer wood yielded slightly better results than those from SIMCA and PLS-DA models. However, the non-linearity of the algorithms used for this

Table 4
Results of the PLS-DA model, cross-validated and predicted values.

PLS-DA MODEL[1]	Prediction results			Cross-validated results			Prediction results		
Class	RMSE$_c$	R$_c^2$		RMSE$_{cv}$	R$_{cv}^2$		RMSEp	R$_p^2$	
Core	0.08255	0.9229		0.0913	0.9059		0.0692	0.8512	
Transition	0.1248	0.8382		0.1378	0.7406		0.2169	0.6666	
Outer	0.1051	0.8782		0.1232	0.8084		0.1289	0.7784	
Confusion table	**Model results**			**Cross-validated results**			**Prediction results**		
	core	transition	outer	core	transition	outer	core	transition	outer
Predicted as core	**170**	0	0	**170**	0	0	**170**	0	0
Predicted as transition	0	**100**	0	0	**85**	10	0	**67**	6
Predicted as outer	0	0	**280**	0	5	**270**	0	3	**294**
Unassigned	0	0	0	0	0	0	0	0	0

Classification rule: prediction strict (0.50) 8LV.
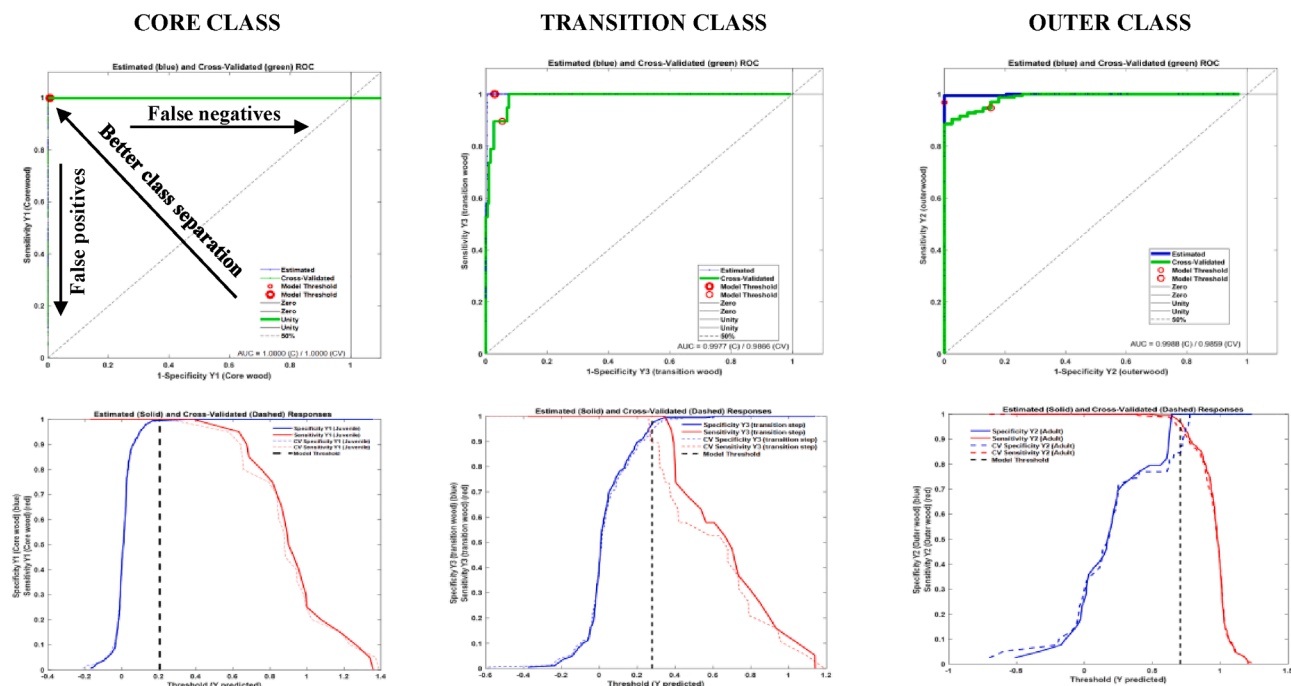
CORE CLASS TRANSITION CLASS OUTER CLASS

Fig. 4. PLS-DA sensitivity/specificity plots and the Receiver Operating Characteristics (ROC) curves.

Table 5
Results of the SVM-DA model, cross-validated and predicted values.

SMV-DA MODEL[1]	Model results			Model CV results			Prediction results		
Class	TPR	FNR	Error	TPR	FNR	Error	TPR	FNR	Error
Core	1.0000	0.0000	0.0000	1.0000	0.0000	0.0000	1.0000	0.0000	0.0000
Transition	1.0000	0.0000	0.0000	0.9330	0.0666	0.0148	1.0000	0.0000	0.0000
Outer	1.0000	0.0000	0.0000	0.9903	0.0096	0.0148	1.0000	0.0000	0.0000
Confusion table	**Model results**			**Model CV results**			**Prediction results**		
	core	transition	outer	core	transition	outer	core	transition	outer
Predicted as core	**170**	0	0	**170**	0	0	**60**	0	0
Predicted as transition	0	**100**	0	0	**99**	2	0	**70**	0
Predicted as outer	0	0	**280**	0	1	**278**	0	0	**300**
Unassigned	0	0	0	0	0	0	0	0	0

Classification rules: kernel function, cost function, gamma function.

method do not allow for scrutinizing the processed IR spectra to find differences among wood classes; thus the SIMCA and PLS-DA models were useful for bands contrasting and categorizing the fingerprint according to the wood type.

3.4. Analysis of IR bands that interact in the classification

The IR bands interacting in the SIMCA, and PLS-DA models were independently analyzed and interpreted to illustrate the chemical features of wood that allow differentiation between core-transition-outer wood. Sixteen bands from the processed IR spectra were selected considering their constant occurrence in the LVs and PCs with maximum discrimination of classes (Table 6).

Selected bands were described according to their vibrational modes using references and descriptions from previous IR studies [34–39]. Finally, they were classified as coming from carbohydrates or/and

Table 6
List of the main bands interacting in the model classification.

Wavenumber (cm^{-1})	Vibration mode	Base group	Core	Transition	Outer
960–940	C-O-C, C-O deformation or stretching	carbohydrates	+	+	+
1030	C = O, C–H, C-O-C, C-O deformation or stretching	carbohydrates			+
1040	C-O-C, C-O deformation	carbohydrates	–	+	+
1060	C = O, C–H, C-O-C, C-O deformation or stretching	carbohydrates	–	+	
1100–1110	C–H, C-O deformation, bending, or stretching	carbohydrates- lignin			+
1170	C = O, C–H, C-O-C, C-O deformation or stretching	carbohydrates	+		
1235	C–H, C-O deformation, bending, or stretching	carbohydrates- lignin		+	
1240	C = O, C–H, C-O-C, C-O deformation or stretching	carbohydrates			+
1270	C = C, C-O stretching or bending	lignin	+		
1380	C = O, C–H, C-O-C, C-O deformation or stretching	carbohydrates			+
1400	C = O, C–H, C-O-C, C-O deformation or stretching 1420–1430 cm1	carbohydrates		+	
1440	C–H, C-O deformation, bending, or stretching	carbohydrates			+
1460	C–H, C-O deformation, bending, or stretching	carbohydrates- lignin	–		
1510	aromatic skeletal C = C	lignin		+	
1560				+	
1590	C = C, C-O stretching or bending	lignin	–		
1640–1647	Absorbed O–H and conjugated C = O	lignin	–	+	

+ Positive scores - negative scores.

lignin, which are the basic chemical components of wood. It must be clarified that the possibility that certain bands assigned to lignin and carbohydrates can originate from several other compounds included in wood, such as extractives and other aromatic compounds.

Most of the peaks identified in the model loadings of *Pinus nigra* correspond to wavenumbers indicating vibrations of carbohydrates-based groups (>56%), then corresponding to lignin-related groups (25%), and finally those that could be seen in both carbohydrates and aromatic compounds (18%). Carbohydrate-related bands exhibited different intensities depending on the wood section, but in general they predominated in the spectra that discriminate the outer wood; specifically the bands at 1030 cm^{-1}, 1100 cm^{-1}, 1240 cm^{-1}, 1380 cm^{-1} and 1440 cm^{-1} were crucial for identification within the models.

It is worth noting the band at 1170 cm^{-1} also corresponding to polysaccharides but that only appears intensified in the core wood spectra (with positive scores), thus establishing itself as a characteristic band of the core wood. Moreover, another band located at 1270 cm^{-1} corresponding to lignin-based groups was representative of core wood, and together with the 1170 cm^{-1} band, they were the only ones with positive discriminant scores in this region, thus suggesting a strong influence of these bands on the predicting spectra of core wood.

On the other hand, the transition wood spectra exhibited a broader variation than core-outer wood in terms of the number and type of representative groups in the fingerprint region. Firstly, the signals belonging to carbohydrates at 1040–1060 cm^{-1} and 1400 cm^{-1} were particularly intense in the loadings that differentiate the transition wood from the other sectors. Also, the bands assigned to groups related to lignin (benzene rings, aromatic rings) were quite intense within this sector, obtaining positive scores in the signals at 1510 cm^{-1}, 1590 cm^{-1}, and 1647 cm^{-1}. Finally, the signal at 1235 cm^{-1} (representing C-O stretching of lignin and xylans) was relatively strong in that spectra; therefore, it can be assumed that there are stronger interactions between xylan groups in the transition wood than in core-outer wood of *Pinus nigra* Arn. Subsp.Salzmannii.

4. Conclusions

The spectrophotometric measurements carried out in the IR region generated interesting results in terms of the discriminative classification of core wood transition or outer wood of *Pinus nigra*, obtaining a reduced group of signals with stronger influence in the prediction and classification of this raw material. The results of the predictive models of woody regions were in general satisfactory, the non-linear SVM-DA model outperformed that of the PLSE-DA and SIMCA methods; however,

the databases require progressive calibration and adjustments in the sensitivity/specificity to increase the reliability of the algorithms generated during calibration and to have an acceptable reliability when validating the method over time. The linear SIMCA and PLS-DA models were useful for bands contrasting and categorizing the IR fingerprint in relation to the core-transition-outer regions. The band assignments of the IR spectra combined with the LVs and PCs allowed to visualize the minors bands that chemically differentiate the woody regions. Carbohydrate-related bands were dominant but with different intensities depending on the wood section, they dominated the spectra that discriminate the outer wood, but for the transition and core wood the spectra were combined with bands representative of lignin and aromatics compounds. This study shows discriminative models from a non-destructive methodology that is relatively fast and with a high correlation coefficient, thus improving the existing methods that are currently in practice for identifying wood quality.

Declaration of Competing Interest

The authors declare that they have no known competing financial interests or personal relationships that could have appeared to influence the work reported in this paper.

Acknowledgements

References

[1] B.J. Zobel, J.R. Sprague, Juvenile wood in forest trees, Springer Science & Business Media, 2012.

[2] M. Dobner, J. Huss, M. Tomazello Filho, Wood density of loblolly pine trees as affected by crown thinnings and harvest age in southern Brazil, Wood Science and Technology 52 (2) (2018) 465–485, https://doi.org/10.1007/s00226-017-0983-9.

[3] A.R. Sastre, Análisis de metodologías para la evaluación de la madera juvenil en la calidad de la madera, Universidad de Córdoba (ESP)), 2019. Doctoral dissertation.

[4] P.R. Larson, Formation and properties of juvenile wood in southern pines: a synopsis, US Department of Agriculture Vol. 129 (2001).

[5] R.D. Burdon, R.P. Kibblewhite, J.C. Walker, R.A. Megraw, R. Evans, D.J. Cown, Juvenile versus mature wood: a new concept, orthogonal to corewood versus outerwood, with special reference to Pinus radiata and P. taeda, Forest science 50 (4) (2004) 399–415.

[6] H. Amarasekara, M.P. Denne, Effects of crown size on wood characteristics of Corsican pine in relation to definitions of juvenile wood, crown formed wood and core wood, Forestry 75 (1) (2002) 51–61.

[7] I. Bobadilla, R.D. Martínez, M. Esteban, D.F. Llana, Estimation of wood density by the core drilling technique, Holzforschung 72 (12) (2018) 1051–1056.

[8] R. Lehnebach, J. Bossu, S. Va, H. Morel, N. Amusant, E. Nicolini, J. Beauchêne, Wood density variations of legume trees in French Guiana along the shade tolerance continuum: heartwood effects on radial patterns and gradients, Forests 10 (2) (2019) 80.

[9] T. De Mil, Y. Tarelkin, S. Hahn, W. Hubau, V. Deklerck, O. Debeir, J. Van Acker, C. de Cannière, H. Beeckman, J. Van den Bulcke, Wood density profiles and their corresponding tissue fractions in tropical angiosperm trees, Forests 9 (12) (2018) 763.

[10] Kita, Y., Mizuno-Tazuru, S., & Sugiyama, J. (2020). Two-dimensional microfibril angle mapping via polarization microscopy for wood classification. In IOP Conference Series: Earth and Environmental Science (Vol. 415, No. 1, p. 012028). IOP publishing.

[11] C. Lu, J. Wu, Q. Jiang, Y. Liu, L. Zhou, Y. You, S. Liu, Influence of juvenile and mature wood on anatomical and chemical properties of early and late wood from Chinese fir plantation, Journal of Wood Science 67 (1) (2021) 1–11.

[12] I. Fundova, T. Funda, H.X. Wu, D. Gomory, Non-destructive wood density assessment of Scots pine (Pinus sylvestris L.) using Resistograph and Pilodyn, PloS one 13 (9) (2018) e0204518.

[13] P. Jacquin, F. Mothe, F. Longuetaud, A. Billard, B. Kerfriden, J.M. Leban, CarDen: a software for fast measurement of wood density on increment cores by CT scanning, Computers and Electronics in Agriculture 156 (2019) 606–617.

[14] J. Gaitan-Alvarez, R. Moya, A. Berrocal, The use of X-ray densitometry to evaluate the wood density profile of Tectona grandis trees growing in fast-growth plantations, Dendrochronologia 55 (2019) 71–79.

[15] A. Ruano, J.L. García de Ceca, J.C. Cabrero, E. Hermoso, Shrinkage pattern assessment for black pine juvenile wood delimitation, European Journal of Wood and Wood Products 80 (1) (2022) 131–138.

[16] M.N. Gebreselassie, K. Ader, N. Boizot, F. Millier, J.-P. Charpentier, A. Alves, R. Simões, J.C. Rodrigues, G. Bodineau, F. Fabbrini, M. Sabatti, C. Bastien, V. Segura, Near-infrared spectroscopy enables the genetic analysis of chemical properties in a large set of wood samples from Populus nigra (L.) natural populations, Industrial Crops and Products 107 (2017) 159–171.

[17] A. Ruano, A. Zitek, B. Hinterstoisser, E. Hermoso, NIR hyperspectral imaging (NIR-HI) and μXRD for determination of the transition between juvenile and mature wood of Pinus sylvestris L, Holzforschung 73 (7) (2019) 621–627.

[18] G. Toscano, Å. Rinnan, A. Pizzi, M. Mancini, The use of near-infrared (NIR) spectroscopy and principal component analysis (PCA) to discriminate bark and wood of the most common species of the pellet sector, Energy & Fuels 31 (3) (2017) 2814–2821.

[19] R. Kitamura, T. Inagaki, S. Tsuchikawa, Determination of true optical absorption and scattering coefficient of wooden cell wall substance by time-of-flight near infrared spectroscopy, Optics Express 24 (4) (2016) 3999–4009.

[20] M. Báder, R. Németh, J. Sandak, A. Sandak, FTIR analysis of chemical changes in wood induced by steaming and longitudinal compression, Cellulose 27 (12) (2020) 6811–6829.

[21] A. Sandak, J. Sandak, M. Riggio, Assessment of wood structural members degradation by means of infrared spectroscopy: an overview, Structural Control and Health Monitoring 23 (3) (2016) 396–408.

[22] O. Faix, Classification of Lignins from Different Botanical Origins by FT-IR Spectroscopy, Holzforschung 45 (s1) (1991) 21–28.

[23] M.J.C.R. Schwanninger, J.C. Rodrigues, H. Pereira, B. Hinterstoisser, Effects of short-time vibratory ball milling on the shape of FT-IR spectra of wood and cellulose, Vibrational spectroscopy 36 (1) (2004) 23–40.

[24] S.M. Moosavinejad, M. Madhoushi, M. Vakili, D. Rasouli, Evaluation of degradation in chemical compounds of wood in historical buildings using FT-IR and FT-Raman vibrational spectroscopy, Maderas. Ciencia y tecnología 21 (3) (2019) 381–392.

[25] A. Rohman, A. Windarsih, E. Lukitaningsih, M. Rafi, K. Betania, N.A. Fadzillah, The use of FTIR and Raman spectroscopy in combination with chemometrics for analysis of biomolecules in biomedical fluids: A review, Biomedical Spectroscopy and Imaging 8 (3–4) (2019) 55–71.

[26] V. Sharma, J. Yadav, R. Kumar, D. Tesarova, A. Ekielski, P.K. Mishra, On the rapid and non-destructive approach for wood identification using ATR-FTIR spectroscopy and chemometric methods, Vibrational Spectroscopy 110 (2020) 103097.

[27] J.I. Fernández-Golfín, M.R. Díez, M.V. Baonza, A. Gutiérrez, E. Hermoso, M. Conde, V. Van den Eynde, Quality and properties of Spanish Laricio Pine (Pinus nigra Arn, Salzmannii). Forest Systems 10 (2) (2001) 311–331.

[28] H. Chen, C. Ferrari, M. Angiuli, J. Yao, C. Raspi, E. Bramanti, Qualitative and quantitative analysis of wood samples by Fourier transform infrared spectroscopy and multivariate analysis, Carbohydrate polymers 82 (3) (2010) 772–778.

[29] M. Bylesjö, M. Rantalainen, O. Cloarec, J.K. Nicholson, E. Holmes, J. Trygg, OPLS discriminant analysis: combining the strengths of PLS-DA and SIMCA classification, Journal of Chemometrics: A Journal of the Chemometrics Society 20 (8–10) (2006) 341–351.

[30] D. Suhandy, M. Yulia, Peaberry coffee discrimination using UV-visible spectroscopy combined with SIMCA and PLS-DA, International journal of food properties 20 (sup1) (2017) S331–S339.

[31] O. Özdikicierler, Chemometric discrimination of Turkish olive oils by variety and region using PCA and comparison of classification viability of SIMCA and PLS-DA, European Food Research and Technology 247 (1) (2021) 157–168.

[32] A. Biancolillo, M. Foschi, M. Di Micco, F. Di Donato, A.A. D'Archivio, ATR-FTIR-based rapid solution for the discrimination of lentils from different origins, with a special focus on PGI and Slow Food typical varieties, Microchemical Journal 178 (2022) 107327.

[33] V. Vapnik, The nature of statistical learning theory, Springer science & business media, 1999.

[34] Hassanien, A. E., & Oliva, D. A. (Eds.). (2017). Advances in soft computing and machine learning in image processing (Vol. 730). Springer.

[35] M. Mukrimin, A.O. Conrad, A. Kovalchuk, R. Julkunen-Tiitto, P. Bonello, F. O. Asiegbu, Fourier-transform infrared (FT-IR) spectroscopy analysis discriminates asymptomatic and symptomatic Norway spruce trees, Plant Science 289 (2019) 110247.

[36] R. Herrera, X. Erdocia, R. Llano-Ponte, J. Labidi, Chemical analysis of industrial-scale hydrothermal wood degraded by wood-rotting basidiomycetes and its action mechanisms, Polymer Degradation and Stability 117 (2015) 37–45.

[37] C.R. Orton, D.Y. Parkinson, P.D. Evans, N.L. Owen, Fourier transform infrared studies of heterogeneity, photodegradation, and lignin/hemicellulose ratios within hardwoods and softwoods, Applied spectroscopy 58 (11) (2004) 1265–1271.

[38] A. Célino, O. Gonçalves, F. Jacquemin, S. Fréour, Qualitative and quantitative assessment of water sorption in natural fibres using ATR-FTIR spectroscopy, Carbohydrate polymers 101 (2014) 163–170.

[39] M.C. Popescu, C.M. Popescu, G. Lisa, Y. Sakata, Evaluation of morphological and chemical aspects of different wood species by spectroscopy and thermal methods, Journal of molecular structure 988 (1–3) (2011) 65–72.